Arabinose oxidation in a fixed bed of extrudates and solid foams containing gold nanoparticles

Simakova, Irina L.; Hachhach, Mouad; Aho, Atte; Eränen, Kari; Wärnå, Johan; Salmi, Tapio; Murzin, Dmitry Yu

Published in:
Chemical Engineering Journal

DOI:
10.1016/j.cej.2023.145659

Published: 15/10/2023

Document Version
Final published version

Chemical Engineering Journal 474 (2023) 145659

Contents lists available at ScienceDirect

Chemical Engineering Journal

journal homepage: www.elsevier.com/locate/cej

Arabinose oxidation in a fixed bed of extrudates and solid foams containing gold nanoparticles

Irina L. Simakova [a], Mouad Hachhach [b], Atte Aho [b], Kari Eränen [b], Johan Wärnå [b], Tapio Salmi [b], Dmitry Yu. Murzin [b,*]

[a] Boreskov Institute of Catalysis, Novosibirsk 630090, Russia
[b] Laboratory of Industrial Chemistry and Reaction Engineering (TKR), Johan Gadolin Process Chemistry Centre (PCC), Åbo Akademi University, 20500 Abo/Turku, Finland

ARTICLE INFO

Keywords:
Sugar oxidations
Gold catalysts
Arabinose
Fixed bed
Extrudates
Aluminum foam
Kinetic modelling

ABSTRACT

Oxidation of arabinose was investigated in a tandem reactor system comprising a fixed bed of gold catalysts supported on extrudates or solid foams and a stirred tank allowing operation under constant pH of 8. Powder catalyst containing 3 wt% Au deposited on γ-alumina was extruded with γ-alumina and attapulgite or sepiolite as a binder or deposited on the solid open-cell aluminum foam after anodic oxidation pretreatment. Alternatively, deposition precipitation of gold with urea from $HAuCl_4$ precursor was done directly on the extruded support or the solid foam.

The presence of gold was essential for catalytic activity which in the applied reactor set-up was strongly limited by mass transfer. Arabinose was rather selectively (ca. 90–95% at full conversion) oxidized to arabinonic acid giving besides arabinolactone other by-products. A mathematical model was developed for the open foam catalyst structures and the extrudates, comprising intrinsic kinetics deduced from batch experiments and the mass transfer within the solid catalyst.

1. Introduction

The biorefinery as a concept, alternative to conventional production of chemicals based on fossil resources, has gained increasing popularity [1–3]. One of the most readily available feedstock – lignocellulose, comprising mainly cellulose, hemicelluloses and lignin, has been considered as a source of bio-based products, such as chemicals, materials and fuels [4–6].

Numerous attempts to synthesize fuels and chemicals from cellulose and lignin have been reported with already several commercial products available on the market, e.g. lignosulfonates, vanillin, ethanol, butanol, carboxymethylcellolose, lignin-based carbon to name a few. Hemicelluloses- branched polymers comprising several sugar monomers, can be easily extracted from lignocellulose in water at moderate temperatures [7,8]. Subsequent hydrolysis of hemicelluloses in the presence of homogeneous or heterogeneous acid catalysts [9–11] results in carbohydrates, which can be further processed. For example, hydrolysis of arabinogalactan, the hemicellulose of the larch tree (*Larix sibirica*), results in a mixture of galactose and arabinose. The latter can be oxidized to the corresponding aldonic acid using either a noble metal, e.g. palladium, platinum or gold.

Supported gold (Au) nanoparticles have been demonstrated to exhibit high catalytic activity, selectivity and stability in oxidation of various sugars [12–15] such as e.g. glucose, galactose and arabinose, giving the corresponding acids, which are widely applied in medicine and cosmetics, as well as food and detergent industries [16]. Different materials, such as ceria, alumina, titania and activated carbon have been used as the supports for catalysts in selective oxidation of various alcohols and sugars allowing to conclude that Au supported on alumina has a high activity in the oxidation of sugars [17]. Oxidation of sugars is typically carried out under mild conditions (50 – 70 °C, pH 6–9, atmospheric pressure) [17].

Oxidation of arabinose on Au catalysts has been extensively studied in the context of the reaction mechanism due to the complex nature of the adsorbed species on the metal surface, including speciation of adsorbed oxygen and its location [15,17–20]. Active gold catalysts typically contain Au nanocrystallites of diameter 2–4 nm, supported on an oxide material. Structure sensitivity in the oxidation reactions

* Corresponding author.
E-mail address: dmurzin@abo.fi (D.Yu. Murzin).

https://doi.org/10.1016/j.cej.2023.145659
Received 13 April 2023; Received in revised form 1 August 2023; Accepted 24 August 2023
Available online 25 August 2023

implies the key role of the gold nanoparticles size among other factors determining catalytic activity [21]. For example, Au particles of ca. 2.5 nm exhibit the highest catalytic performance in arabinose oxidation [21].

Activation of oxygen on gold has been debated even if there is a general consensus on energetically unfavorable activation and dissociation of dioxygen on gold single crystals [22] is that and Au atoms at the interface between the Au cluster and the oxide support are often considered as the sites for oxygen activation and dissociation [22–25], while the substrate can be activated by adsorption on the Au nanoparticle per se.

Conventional methods for processing of carbohydrates such as oxidation, as well as hydrogenation [26] and isomerization [27] are mainly limited to batch and semi-batch processes in the presence of finely dispersed catalyst particles, thus essentially being limited to discontinuous production technology. Attempts along the recent years to establish continuous sugar hydrogenation processes using fixed bed reactors have been rather successful even though the need to use larger catalyst particles in beds inevitably results in heavy internal mass transport limitations. In the case of sugar hydrogenation over carbon supported ruthenium catalysts a viable option is to use structured catalysts, for example open foams [28,29]. This is related to limited shaping opportunities of carbon, which was reported as an optimal support for ruthenium. Contrary to hydrogenation, oxidation of sugars as mentioned above, can proceed efficiently over gold supported on alumina, which is a conventional catalyst support and can be exposed to different type of shaping, e.g. by extrusion and 3D printing.

There is a limited experience in conducting oxidation of sugars in continuous fixed bed reactors. Bitter and co-workers described oxidation of sodium galacturonate to disodium galactarate under alkaline conditions [30] as well as oxidation of glucose and galactose without adding a base [31] over Au supported on titania with the size of granules in the range of 0.5–0.65 mm. The substrate scope in the experiments without addition of a base was extended to include glucuronic and galacturonic acids [31]. These experiments were conducted at an elevated pressure of 10 bar at 40–100 °C with 0.1 M aqueous solutions of the sugars for one hour time on stream (TOS) with the solution feed rate 10 mL/min. In that studies [30,31] pH was not adjusted during the reaction, contrary to a batch operation when experiments are conventionally done at a constant pH. In fact, pH adjustment in a batch operation is required as otherwise because of acid formation the pH is drifted during the experiment substantially changing the reaction rate.

Another example of glucose oxidation in a trickle bed reactor includes utilization of a gold catalyst based on a micro-mesoporous carbon with the grain dimensions exceeding 600 μm [32]. Also here no pH adjustment was done along the reactor bed. Complete conversion was reported for the liquid flow rate of 20 mL/h at 70 °C, 1 bar of oxygen and the residence time of 1.2 min calculated as the ratio between the volume of the catalyst bed and the liquid flow rate. The initial glucose solution (5 wt%) has the pH of 13.5. Besides gluconic acid substantial amounts of by-products (glycolic and formic acids and especially fructose) were reported depending on the operation conditions, namely elevated temperature (i.e. 90 °C), high gas flow rates or initial glucose concentration (i.e. 10 wt%).

In the current work, oxidation of arabinose was performed in a fixed bed reactor using shaped catalyst bodies to avoid high pressure drop inevitable with catalyst powders. Sepiolite ($Mg_2H_2SiO_9xH_2O$, Sigma-Aldrich) and attapulgite ($(Mg,Al)_2Si_4O_{10}(OH)\cdot4(H_2O)$) were selected as binders based on previous studies on transformations of fine chemicals over shaped catalysts [33,34].

Oxidation of arabinose previously performed on gold nanoparticles indicated that the reaction time in a batch reactor with 100 mL of 2 wt% sugar solutions at ca. 70 °C and pH 8 with 1 g of catalyst is typically ca. 2 h to achieve full conversion. Due to external and internal mass transfer limitations present in shaped catalyst bodies, which are in the mm range and do not exhibit the egg-shell concentration profiles, the catalyst effectiveness factor (the ratio between the observed rate to the rate in the kinetic regime) is expected to be less than unity.

A rather low conversion per pass could be thus anticipated in the case of the fixed bed reactor with catalyst extrudates. Subsequently the fixed bed reactor operated in the circulation mode allowing the adjustment of pH after each pass. A similar operation mode was applied for oxidation of lactose to lactobionic acid sodium salt in a pilot monolith reactor with a Pd/C catalyst on a cordierite monolith when pH was adjusted by suppling a sodium hydroxide solution to a gas–liquid separator located downstream a catalytic reactor [35].

This work is therefore focused on developing shaped catalyst bodies in the form of extrudates and metallic bodies, deposition of gold onto them and performing oxidation of arabinose in a set-up with a fixed bed reactor allowing a low conversion per pass and a recycling system with a stirred tank to which sodium hydroxide is added to avoid the pH drift.

Due to similarities in oxidation of sugars it is expected that knowledge in scaling up of arabinose oxidation can be transferred to oxidation of mono- and even disaccharides (e.g. lactose).

2. Experimental section

2.1. Catalysts preparation

Two strategies were used for the catalyst preparation. The gold on γ-alumina catalysts were either formed by extrusion using 3 wt%Au/γ-alumina in the powder form together with γ-alumina and a binder (sepiolite or attapulgite) also in the powder form. Alternatively, the extrudates were prepared just with sepiolite and alumina and then deposition of gold was done by precipitation. Both methods were also applied for the preparation of structured catalysts using aluminium foam as the base.

For the preparation of Au supported catalysts C1 and C2 (2 or 3 wt% of Au respectively), the deposition–precipitation method with urea described previously [36] was used. A 1.6×10^{-3} M aqueous solution of $HAuCl_4$ with urea (0.21 M) was mixed with Al_2O_3 as a powder followed by heating at 81 °C for 4 h, which is a typical procedure for deposition precipitation with urea. After filtration, the catalyst was washed with distilled water and then additionally with a 12 M NH_4OH solution to remove the excess chloride after the gold deposition. Thereafter, the catalyst was washed with water, filtered and dried at room temperature for 24 h. This was followed by calcination in air at 350 °C (2 °C/min).

Alumina (VGL-25, UOP Versal) as a support and sepiolite ($Mg_2H_2SiO_9xH_2O$, Sigma-Aldrich) or attapulgite ($(Mg,Al)_2Si_4O_{10}(OH)\cdot4(H_2O)$, Sigma-Aldrich) as a binder were dried overnight at 100 °C and physically mixed in the mass ratio = 70:30. As an organic binder methylcellulose was used to control the rheological properties of the extrusion paste with the mass ratio of 1/100 to the mixture of alumina and an inorganic binder. The extrudates C3-C5 were fabricated in a cylindrical shape using the prepared paste consisting of the alumina support and a binder along with the catalyst C2. The diameter of extrudates (i.e. 1.4 mm or 1.8 mm) was regulated using either 1.5-mm and 1.8 mm diameter-hole die plate. The extruder (TBL-2, Tianjin Tianda Beiyang Chemical Co. Ltd., China) was driven by a rotational velocity of 1400 rpm.

In the case of C3-C5 catalysts, the extrudates were dried in an oven at 100 °C overnight, calcined at 350 °C for 4 h in a muffle oven, and cut to a length of ca. 0.6–1.0 cm.

The extrudates C6 were prepared just with alumina and sepiolite in the same ratio (70:30) as other catalysts. Thereafter, gold was deposited on the extrudates using the deposition–precipitation method with urea as described previously. A 1.6×10^{-3} M aqueous solution of $HAuCl_4$ with urea (0.21 M) was circulated through the bed of extrudates at 81 °C for 4 h using an external pump. The same procedure was used for the extrudates. After deposition–precipitation the catalyst was washed with distilled water and then a 12 M NH_4OH solution to remove the excess of chloride. Similar to the preparation of the powder catalyst after drying

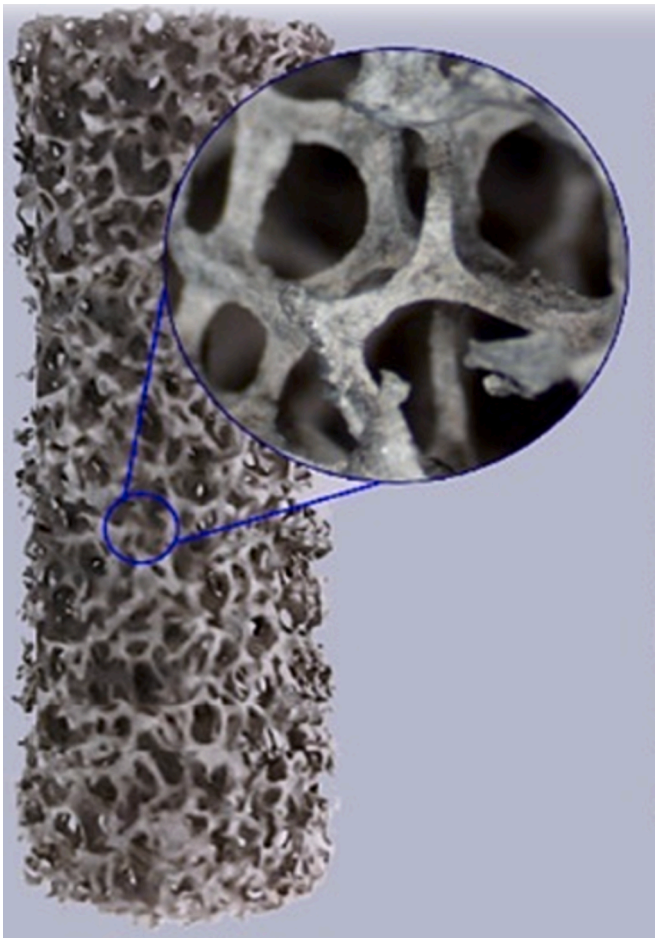

Fig. 1. Aluminium foam used as the support for deposition–precipitation with urea.

at room temperature for 24 h, the extrudates were calcined in air at 350 °C (2 °C/min).

For the preparation of C7 catalyst aluminium foam sheets (Good-Fellow Cambridge Ltd.) with 5 PPI cell density were used. First cylinders with an average diameter of 11 mm and a length of 33 mm were cut (Fig. 1) and washed 15 min with water and acetone in an ultrasonic bath followed by drying for 2 h at 70 °C and overnight at room temperature.

Prior washcoating, a thin oxide layer was formed via an anodization procedure reported in detail previously along with the corresponding SEM [37] and enhanced by additional hydrothermal treatment at 330 °C during 12 h followed by calcination in air by heating to 250 °C at the heating rate 1 °C/min for 2 h and then to 450 °C at 1 °C/min for 2 h.

On the modified foam (0.684 g) catalyst C1 (2 wt% Au/Al_2O_3, 0.137 g) was deposited from a suspension containing also attapulgite (0.042 g) as well as 0.005 g methylcellulose. After deposition of the catalytic phase and drying, the catalyst was calcined at 300 °C for 1 h to decompose methylcellulose.

C8 catalyst was prepared similarly to the catalyst C6 by homogeneous deposition–precipitation of $HAuCl_4$ and urea on the anodized foam preliminary washcoated by alumina (0.5348 g including 0.119 g of alumina layer) using aluminium foam sheets with 5 PPI cell density.

Thus the tested catalysts included extrudates of different length and a binder made with a ready- made gold containing catalyst; extrudates when gold was introduced by precipitation from a gold-containing precursor; anodized aluminium foam onto which the ready-made catalyst was coated or alternatively gold was deposited by homogeneous precipitation. The set of catalysts thus comprised materials with a thin catalyst layer (foams) as well as extrudates when the mass transfer limitations were anticipated due to the size of extrudates.

Characterization of the gold on alumina catalyst has been reported previously [36] giving the gold particle size ca. 2.5 nm.

2.2. Catalysts characterization

The mechanical strength of the shaped catalyst was measured by the crush tester (SE 048, Lorentzen & Wettre) for 4–6 extrudates in the horizontal and vertical positions.

The metal particle size, and their location in extruded catalysts were analyzed by transmission electron microscopy with JEOL JEM-1400Plus. Studies of the microstructure and morphology of the samples were performed using a double-corrected transmission electron microscope ThemisZ (Thermo Fisher Scientific) in high-angle annular dark-field/scanning transmission electron microscopy (HAADF/STEM) and high-resolution transmission electron microscopy (HRTEM) modes with an acceleration voltage of 200 kV. Collection of images was performed with a CCD Ceta 16 matrix. The device was equipped with an energy dispersion spectrometer of X-ray radiation (SuperX) equipped with a semiconductive Si detector with an energy resolution of 128 eV. The samples were deposited on holey carbon holders and supported on Cu grids using an ultrasound device.

The textural properties such as the specific surface area, porosity and the pore size distribution were measured with nitrogen physisorption using Micromeritics 3Flex-3500 device, showing that there were no changes in the surface area of the coated catalysts after the coating procedure. The surface area of the gold/ alumina catalyst was 200 m^2/g with the pore volume of 0.5 cm^3/g and the average pore diameter of 10 nm.

Table 1
Prepared catalysts for oxidation of arabinose and experimental conditions.

code	Brief description	Gold loading in final catalysts, wt%	Catalyst amount, g	Arabinose conc., M	Solution volume, mL	Solution flow rate, mL/min	Rate, M m^3/(g_{Au} min)
C1	2 wt%Au/Al_2O_3 powder	2	–	–	–	–	
C2	3 wt%Au/Al_2O_3 powder	3	0.1	0.133	150	Batch	$1.1\ 10^{-4}$
C3	3 wt%$Au\text{-}Al_2O_3$ /alumina/sepiolite Extrudates 1.4 mm	0.166	2.36	0.133	250	234.4	$5.3\ 10^{-6}$
C4	3 wt%Au/Al_2O_3 /alumina/sepiolite /Extrudates 1.8 mm	0.207	2.85	0.133	250	234.4	$4.3\ 10^{-6}$
C5	3 wt%Au/Al_2O_3 /alumina/attapulgite Extrudates 1.4 mm	0.5	1.99	0.133	250	181.8	$2.6\ 10^{-6}$
C6	Alumina/sepiolite /Extrudates 1.8 mm. Homogeneous precipitation of $HAuCl_4$	n.d.	0.50	0.0655	250	181.8	$1.8\ 10^{-6}$
C7	2 wt%Au/Al_2O_3 attapulgite/ Aluminum open cell foam PPI 5	0.2	0.79	0.0655	250	121.1	$1.04\ 10^{-5}$
C8	Aluminum open cell foam PPI 5 Homogeneous precipitation of $HAuCl_4$	1.5	0.54	0.0655	250	121.1	$2.8\ 10^{-6}$

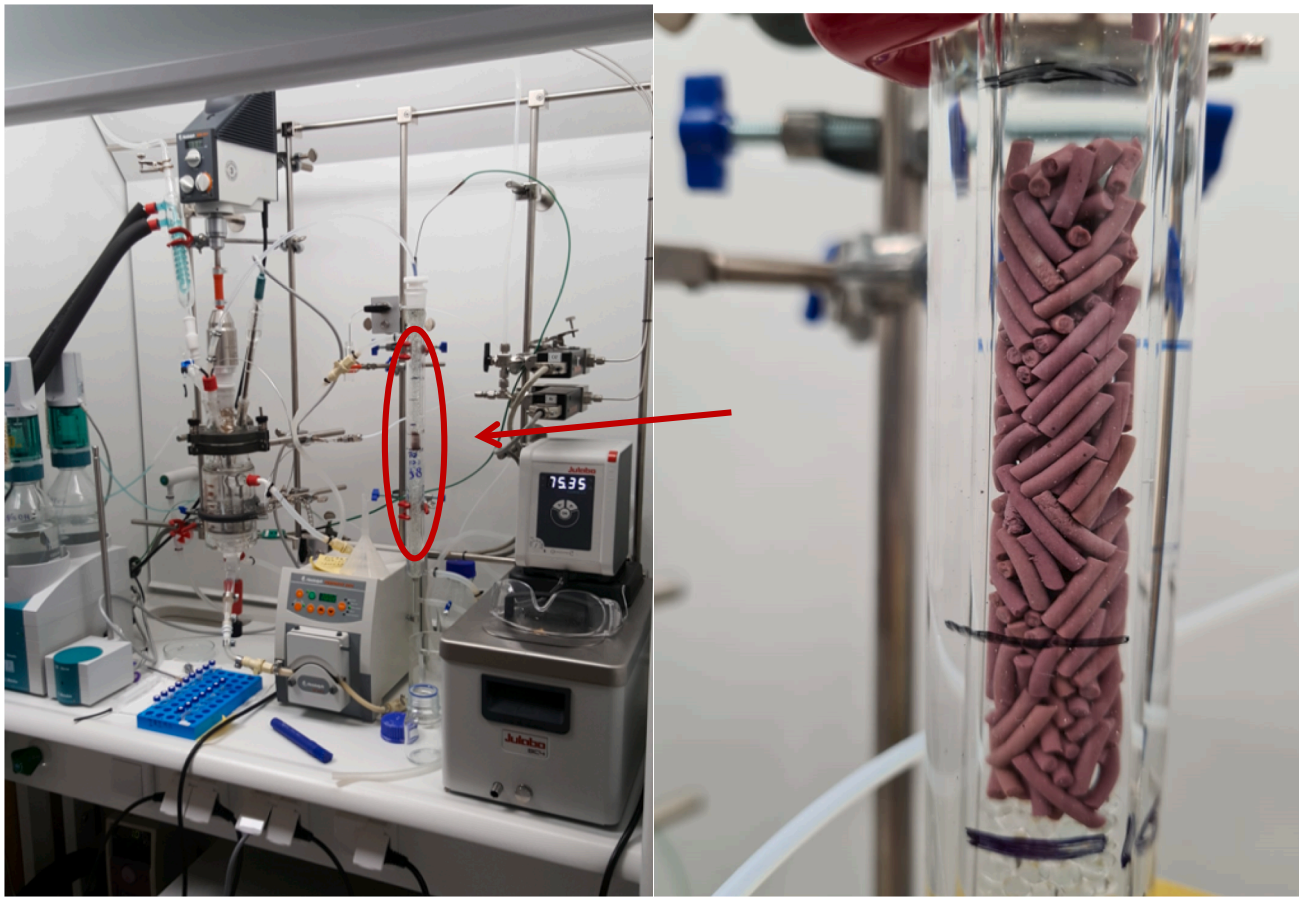

Fig. 2. Recyle reactor set-up and catalyst bed.

2.3. Catalytic experiments

Oxidation of arabinose in a semi-batch mode under a constant flow of oxygen and thus constant concentration of dissolved oxygen was performed in a laboratory-scale glass reactor equipped with an efficient mechanical stirrer and a heating jacket. A short description of the conditions is presented in Table 1. A Brooks 5850S device was used in order to control and adjust the gas feed (150 mL/min). Temperature (70 °C) was controlled by two thermocouples placed inside the tank reactor, to which NaOH was added, and also on the top of the fixed-bed reactor. The temperature difference was ca 0.02 °C pointing out on the isothermal operation without temperature gradients. The pH (8) was controlled using a Metrohm Titrando 907 device equipped with a Metrohm Unitrode electrode. A particle size less than 65 μm and efficient stirring (1000 rpm) were used to suppress the internal and external mass transfer limitations in the catalyst pores. The liquid volume was 150 mL and the concentration of aqua L-arabinose (Sigma-Aldrich, ≥99%) solution was equal to 0.133 M, while a lower concentration was used for C6-C8 catalysts due to less available metal catalyst amounts for testing. The pH control was carried out using 1 M NaOH. The samples were periodically withdrawn from the liquid phase during the experiments and the concentration profiles of the reactants.

Experiments with a fixed bed of catalyst were done circulating the aqua L-arabinose solution (0.067 M and 0.133 M) (Table 1) through the bed of extrudates (Fig. 2) or the open-cell foams.

The liquid was circulating upflow through the fixed bed reactor containing extrudates followed downstream by the continuous stirred tank, i.e. the same vessel, which was used for batch experiments. The rationale for such reactor arrangements is the easiness of adjusting pH during the reaction, as this is done in the same way as in batch operation because of low conversion levels per pass. In an alternative case when activity would be very high giving a high conversion per pass, pH gradients might appear along the fixed bed reactor requiring multiple points of alkali injection.

The reaction products were monitored using high performance liquid chromatography (VWR Hitachi Chromaster) equipped with a 300x7.8 mm Bio-Rad Aminex HPX-87C column and a RI detector (VWR Hitachi Chromaster 5450). The temperature of the column was 80 °C and the flow rate of 0.6 mL/min using 1.2 mM $CaSO_4$ as an eluent, operating in the isocratic mode, and resulting in a column backpressure ranging between 65 and 70 bar. The injection volume of the investigated sample was 10 μl.

3. Results and discussion

3.1. Characterization of catalysts by transmission electron microscopy

Differently prepared gold bearing catalysts such as C5, C6 extrudates as well as C7 and C8 foams were studied by transmission electron microscopy (TEM) and high angle annular dark field scanning transmission electron microscopy (HAADF-STEM) in order to determine the morphology and gold metal particle size (Fig. 3). To elucidate a possible effect of reaction media TEM data of spent C7 sample were compared with that prior to the reaction. The HRTEM study (Fig. 3) shows that gold nanoparticles of the rounded shape were uniformly distributed on the catalyst surface of C5, C6, C7 and C8 spent samples. The mean gold nanoparticle size for the spent catalysts increased in the sequence C6 ~ C5 < C7 < C8 being 4.1, 4.2, 5.2 and 5.8 nm, respectively. No highly enriched areas with elevated local concentration of gold clusters were observed. Spent C5 extrudates prepared from 3% Au/Al_2O_3 powdered

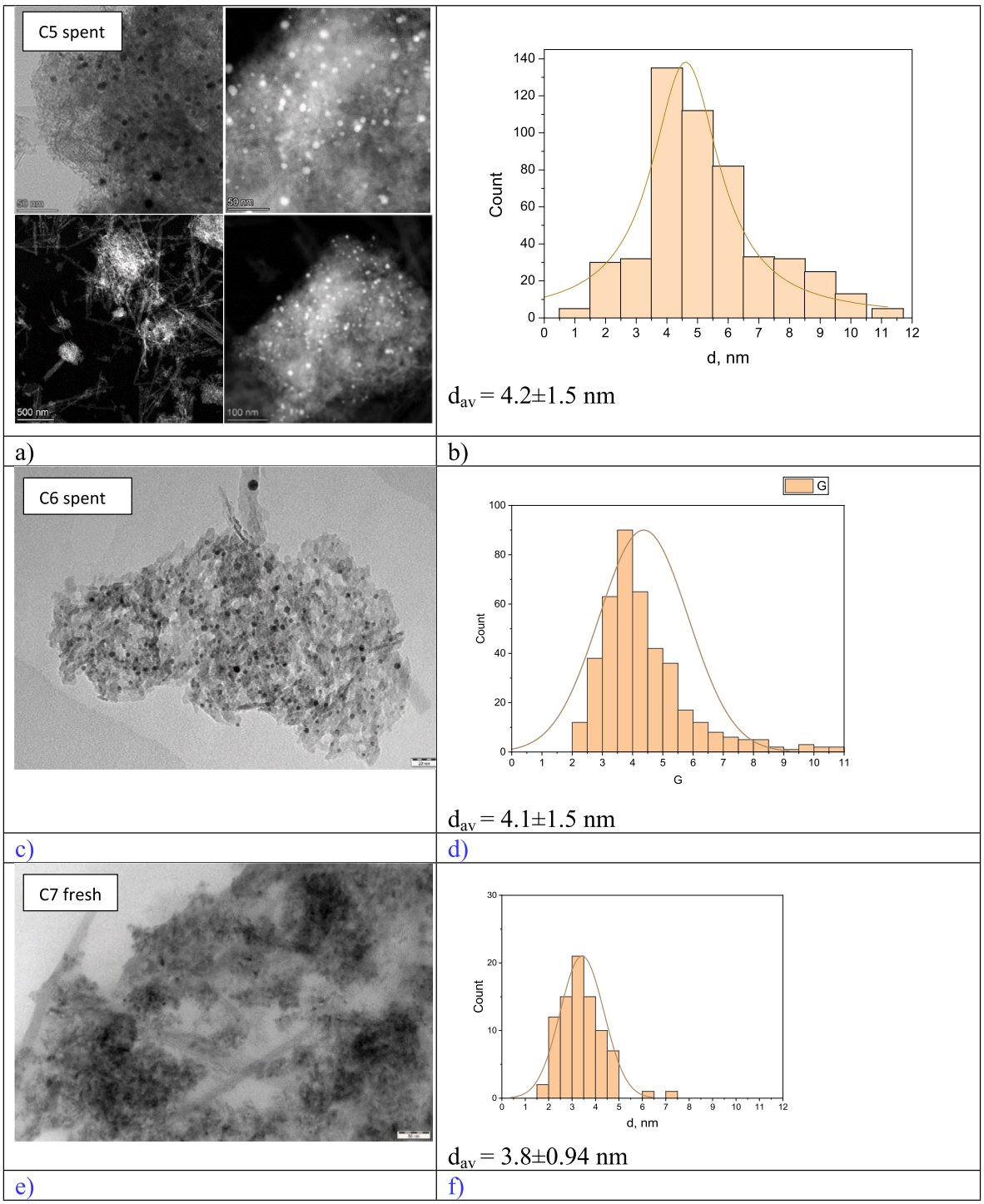

Fig. 3. TEM micrographs of the studied Au catalysts - a) HRTEM and HAADF-STEM images of C5 spent catalyst, b) histogram of particle size distribution for C5 spent catalyst, c) HRTEM image of C6 spent catalyst, d) histogram of particle size distribution for C6 spent catalyst, e) HRTEM image of C7 fresh catalyst, f) histogram of particle size distribution for C7 fresh catalyst, g) HRTEM image of C7 spent catalyst, h) histogram of particle size distribution for C7 spent catalyst, i) HRTEM image of C8 spent catalyst, j) histogram of the particle size distribution for C8 spent catalyst.

catalyst synthesized by homogeneous precipitation and mixing with the attapulgite binder for shaping exhibited comparable gold nanoparticle dispersion as spent C6 extrudates prepared from alumina and sepiolite (7/3) followed by homogeneous precipitation of gold by a similar way.

Both C5 and C6 extrudates are characterized by more dispersed gold nanoparticles compared to the spent C7 and C8 foamed catalysts prepared by either coating aluminium foam with the mixture of 3% Au/Al_2O_3 powdered catalyst and attapulgite (C7), or by coating aluminium foam with the mixture of Al_2O_3 and attapulgite followed by deposition of gold by homogeneous precipitation (C8). Interestingly despite mild reaction conditions (70 °C and 1 bar) the reaction media affected Au nanoparticle size changing from 3.8 to 5.2 nm by 37% during arabinose oxidation (Fig. 3 c-f). Taking into account that for the initial powdered 3% Au/Al_2O_3 with the average Au particle size of ca. 2.8–3.0 nm the size

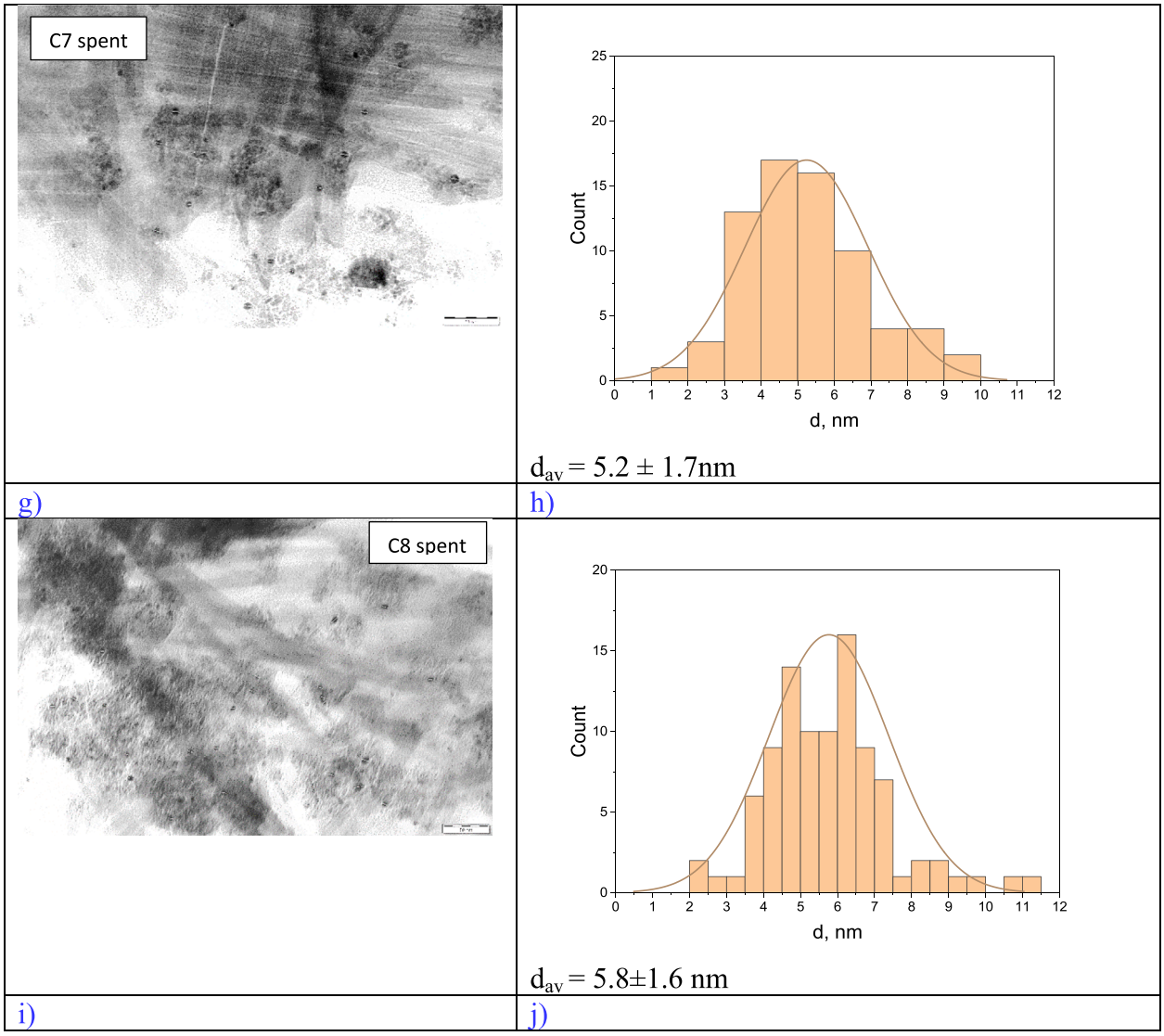

Fig. 3. (*continued*).

increased after reaction to 3.8–4.2 nm, the effect of the reaction media was similar for extruded and structured catalysts.

Note that in general, the deposition precipitation with urea using circulation of the gold precursor solution across the open cell foam could result in the bigger size of the gold particles compared to that in the powder catalyst and less homogeneous distribution of gold compared to the extrudates prepared using powdered Au catalyst. In the case of open-cell foams deposition of the active phase was done either by washcoating with the Au on alumina powder catalyst (C7 catalyst) or alternatively by deposition precipitation with urea using circulation of the gold precursor solution through the open cell foam washcoated with γ alumina foam (C8 catalyst). Such circulation, apparently not needed in the former method, influenced the size of gold clusters. Namely, deposition precipitation of gold on a metallic foam after washcoating first with a gold free γ alumina powder, gave a somewhat lower gold dispersion (Fig. 3 g, h).

For C7 catalyst the thickness of the washcoat layer can be calculated as the volume of the deposited phase divided by the geometrical area of the foam. Taking the bulk density of the suspension and foams as 0.6 and 1 g/cm^3, respectively, the geometrical area for the 5 PPI foam of 500 m^2/m^3 increasing twofold after anodization, the nominal washcoating thickness would be 90 μm, which is very close to the size of the particles in the suspension prior to coating.

Table 2
Average mechanical strength of extrudates in vertical and horizontal positions.

No.	Sample	Mechanical strength (vertical), MPa	Mechanical strength (horizontal), MPa
	C5 catalyst (d = 1.4 mm, binder attapulgite)$_{fresh}$	4.1 ± 0.1	1.2 ± 0.01
2	C4 catalyst (d = 1.8 mm, binder sepiolite)$_{spent}$	Not measured	1.2 ± 0.01
3	Attapulgite [33]	16.3 ± 1.6 (V)	7.7 ± 0.8 (H)
4	Sepiolite [33]	5.6 ± 0.6 (V)	3.5 ± 0.4 (H)

3.2. Mechanical strength

The results of mechanical strength measurements, giving the values of 1.2 ± 0.01 MPa and 4.1 ± 0.1 MPa respectively, for fresh C5 catalyst (d = 1.4 mm, binder attapulgite) and 1.2 ± 0.01 MPa for the C4 spent catalyst (d = 1.8 mm, binder sepiolite) in the horizontal position, are presented in Table 2.

As a comparison, pure attapulgite/sepiolite extrudates of d = 1.4 mm exhibited mechanical strength 7.7 ± 0.8/3.5 ± 0.4 in the horizontal position and 16.3 ± 1.6/ 5.6 ± 0.6 in the vertical position for attapulgite and sepiolite, respectively.

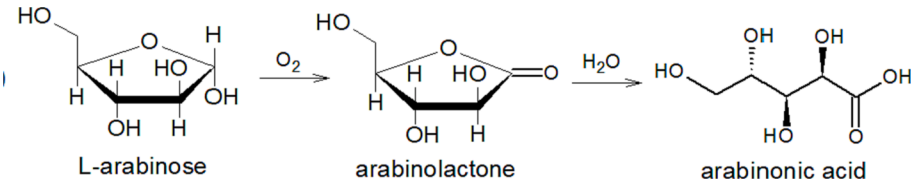

Fig. 4. Main pathways in selective oxidation of arabinose over gold catalysts.

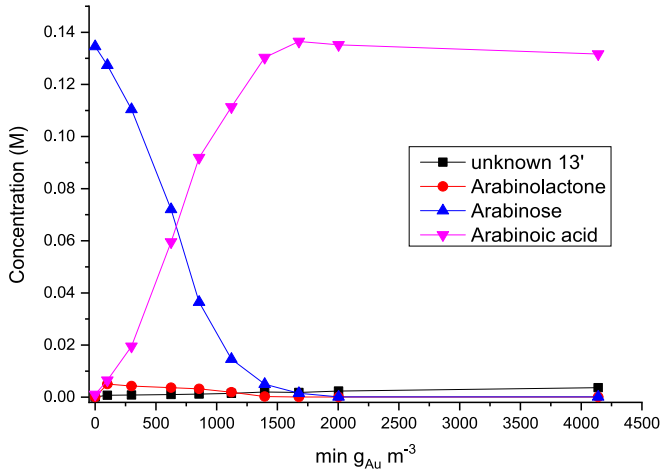

Fig. 5. Oxidation of arabinose over powder 3 wt% Au/alumina (C2) in a semi-batch mode at 70 °C, pH 8, P_{O2} = 1 bar, $C_{0,\ arabinose}$ = 0.133 M.

3.3. Catalytic activity and selectivity

Selective oxidation of arabinose (Fig. 4) over a powder gold on alumina catalyst (C2) carried out isothermally at atmospheric pressure in aqueous phase in semi-batch mode was very selective to the corresponding aldonic acid (Fig. 5) with the final selectivity close to 98%.

The catalytic data were rather similar to the previously reported results obtained in the kinetic regime in the absence of the liquid-to-solid mass transport limitations and intraparticle diffusion limitations [17,19,20]. The main difference was some marginally pronounced S-shaped behavior as well as formation of an unknown compound with the retention time in HPLC 13 min. Presence of another unknown compound at 16 min of retention time (Figure S1) was observed in all experiments with extrudates and open cell foam catalysts. Interestingly, the formation of these compounds increased with conversion.

Previously [38] it has been demonstrated that formation of these unknown compounds, different from arabinolactone and ribulose, can be partially suppressed at elevated oxygen concentrations. When the product peak areas are plotted against each other (not shown) their formation follows the parallel paths. NMR [38] analysis confirmed formation of lower carbon number products (e.g. 2- and 3-hydroxypropionic acid) indicating that the unknown products most probably result from *retro*-aldol condensation or similar reactions leading to C2 and C3 alcohols, diols and hydroxyacids in sugar transformations reported previously [39]. The response factors of the unknown compounds were considered to be the same as for arabinolactone leading to a mass balance closure of ca. 95–97%.

Results of experiments in the tandem reactor system with the C3 catalyst with and without normalization are presented in Figure S2, while Figs. 6 and 7 contain only normalized data for extrudates and foams, respectively to facilitate a comparison between experiments performed with somewhat different amounts of catalyst and gold loadings.

Fig. 8 displays an overview of the experiments with extrudates and foams and compares data in the batch reactor using the normalized time with oxidation of arabinose in the fixed bed.

It can be clearly seen that the observed rate was much higher in the batch reactor with the powder catalyst implying presence of mass transfer limitations in case of the catalyst extrudates.

It should be also noted that the tested catalysts were stable against leaching as confirmed by ICP analysis of the liquid phase demonstrating absence gold in the concentrations above the detection limit (0.003 mg/l). Such results indicate adequate adhesion of the coatings.

As revealed by Fig. 8, a high sugar conversion can be achieved after a prolonged reaction time (20–24 h) in the fixed bed reactor with almost zero order kinetic curves. Among the extrudates, the highest reactivity was exhibited by the C3 catalyst with sepiolite as the binder and the dimeter of 1.4 mm. C5 catalyst with the same diameter (Table 1), where attapulgite was applied as a binder displayed a lower activity. It should be noted that the catalyst C4 with thicker extrudates (Table 1) was as expected less active than C3. The difference between attapulgite and sepiolite, which are both phyllosilicates with continuous two-dimensional tetrahedral sheets, can be tentatively ascribed to higher specific surface area of sepiolite exhibiting also a higher cation exchange capacity and a large channel diameter (0.37 × 1.06 nm vs 0.37 × 0.64 nm for attapulgite).

Because the C3-C5 catalysts were prepared using the same 3 %Au/alumina powder catalyst the intrinsic activity of gold *per se* was the same in these materials. On the contrary, C6 catalyst was prepared by homogeneous deposition–precipitation of gold from its precursor in the presence of urea. It is visible from Fig. 8 that the reaction rate deduced from the slope of the curve is lower than for the counterparts, even if the size of gold clusters is similar as verified by HRTEM. At the same time the cluster size distribution is evidently broader, thus presumably such large clusters are not efficient in oxidation of sugars know to be a structure sensitive reaction. A similar conclusion can be made for catalyst C8.

Synthesis of shaped catalysts by extrusion of gold on alumina as a powder along with the binder inevitably results in presence of mass transfer limitations, as because of the preparation method the active catalytic phase is distributed more or less uniformly in the extrudates.

Contrary to this, washcoating with the ready made catalyst has an advantage of keeping a small washcoating thickness (90 μm) minimizing the influence of internal mass transfer. In addition the size of gold clusters remains resulting in the catalyst (C7) with the second highest activity. Alternatively, deposition precipitation of gold on a metallic foam after washcoating with γ -alumina powder led to a somewhat larger gold cluster size giving a catalyst which was not very active (Fig. 7b).

As mentioned above selectivity to arabinonic acid at close to full conversion was somewhat lower than in the oxidation of arabinose in a stirred tank reactor, being still rather high. Dependence of selectivity as a function of conversion for the studied catalysts is illustrated in Fig. 9 confirming that apart from C3 and C5 all other catalysts including C7 displayed the final selectivity of 95–96% at the conversion level exceeding ca. 80%. Selectivity to the acid was increasing with conversion. This typically indicates a consecutive nature of the reaction network comprising lactone as an intermediate, which is in line with the kinetic curves (e.g. Figs. 6 and 7). An alternative explanation will be related to less prominent generation of the unknown products as the reaction progresses. Note that the initial arabinose concentration did not

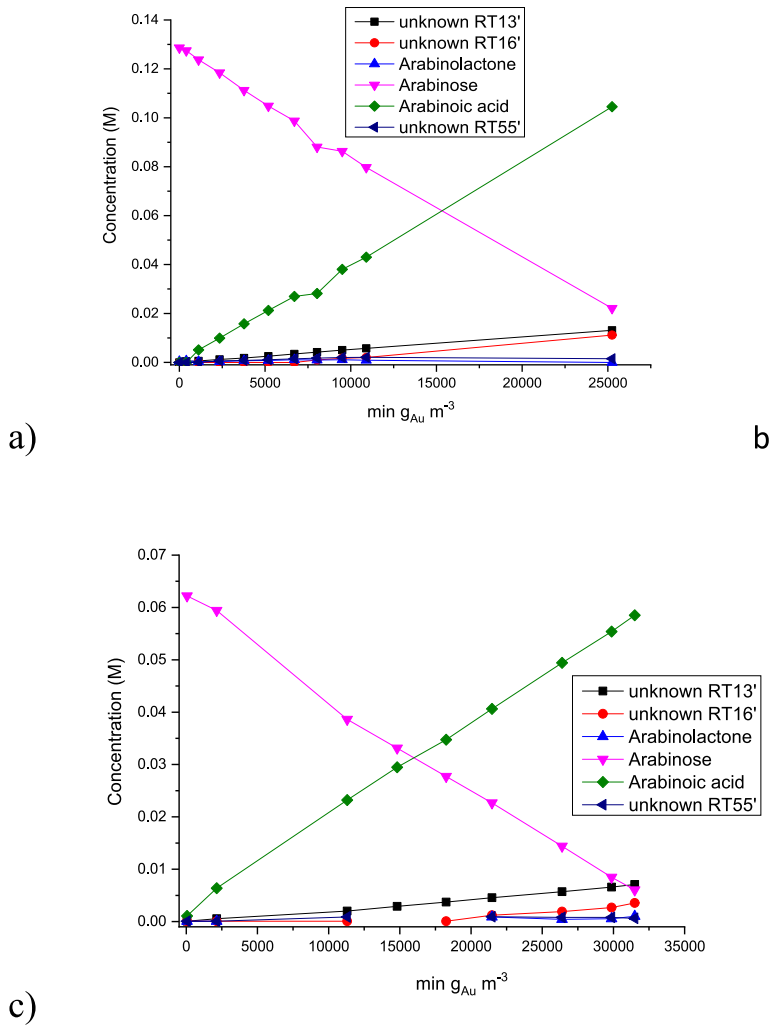

Fig. 6. Kinetic curves for arabinose oxidation in the tandem reactor system vs normalized time for extruded a) C4 (sepiolite binder, 1.8 mm extrudates, coating with the gold catalyst), b) C5 (attapulgite binder, 1.4 mm extrudates, coating with the gold catalyst), c) C6 (sepiolite binder, 1.8 mm extrudates, gold deposition on extrudates) catalysts. Conditions: 70 °C, pH 8, $pO_2 = 1$ bar, $C_{0,\ arabinose} = 0.133$ M. Other details are given in Table 1.

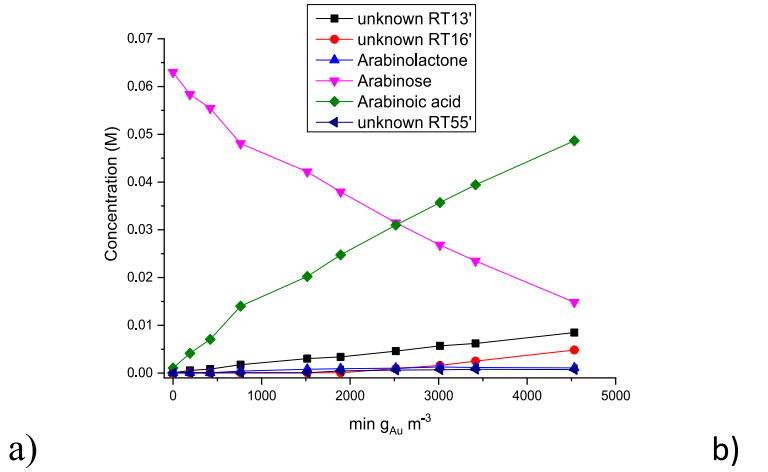

Fig. 7. Kinetic curves for arabinose oxidation in the tandem reactor system vs normalized time for open cell foam a) C7 (Al foam, coating with the gold catalyst), b) C8 (Al foam, gold deposition on foams) catalysts. Conditions:70 °C, pH 8, $pO_2 = 1$ bar. Other details are given in Table 1.

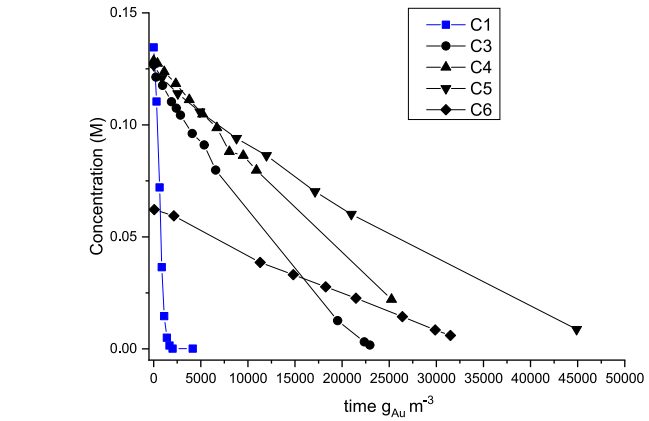

a)

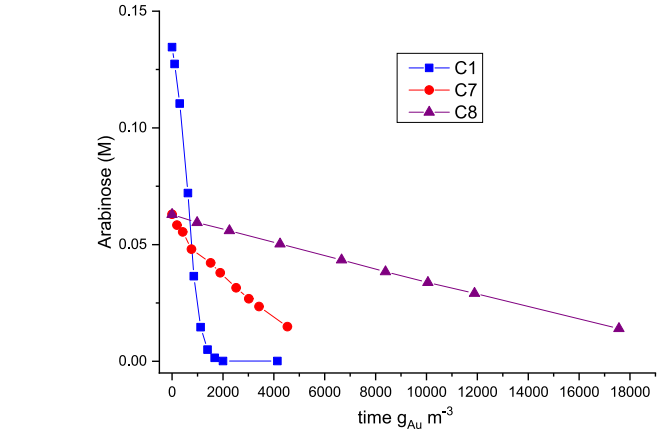

b)

Fig. 8. Comparison of arabinose oxidation in a batch reactor with the tandem reactor system using normalized time a) extrudates, b) open-cell foams. Conditions: 70 °C, pH 8, $pO_2 = 1$ bar, $C_{0,\ arabinose} = 0.133$ M for C2-C5 catalysts, $C_{0,\ arabinose} = 0.067$ M for C6-C8 catalysts. Other details are given in Table 1.

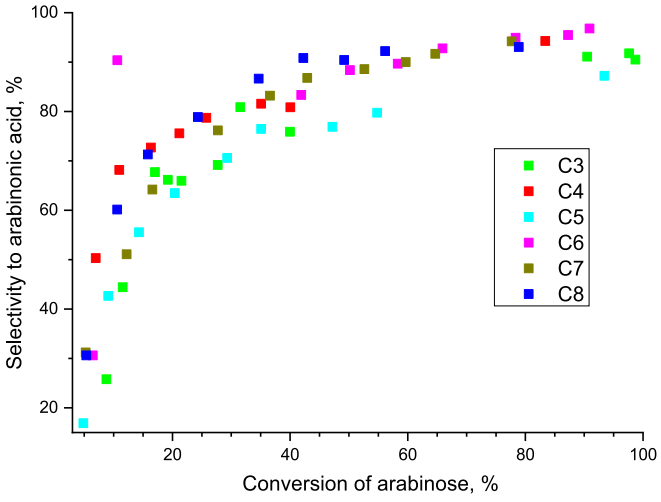

Fig. 9. Selectivity to arabinonic acid vs arabinose conversion in the tandem reactor system. Conditions: 70 °C, pH 8, $pO_2 = 1$ bar, $C_{0,\ arabinose} = 0.133$ M for C2-C5 catalysts, $C_{0,\ arabinose} = 0.067$ M for C6-C8 catalysts. Other details are given in Table 1.

affect noticeably dependence of selectivity to arabinonic acid vs. arabinose conversion (Fig. 9).

3.4. Modelling and simulations

3.4.1. Rate equations

Similar rate equations as presented in our previous publications are used [20,38]. They are based on the hypothesis of molecularly adsorbed oxygen being the active species in the oxidation process and the surface reaction between adsorbed oxygen and arabinose is the rate determining step. The adsorption of arabinonic acid was neglected. These assumptions give the following kinetic expression for the main reaction, formation of arabinonic acid

$$r_1 = \frac{k_1 C_A C_{O2}(a)^2}{(1 + K_A C_A + K_O C_{O2})^2} \quad (1)$$

Where r is the reaction rate, a is the activity function reflecting potential deactivation (equal to unity in the current case), k_1 is a merged rate parameter comprising the kinetic constant of the surface reaction step and the adsorption parameters of oxygen K_O and arabinose K_A.

For the formation of arabinolactone the rate equation is

$$r_2 = \frac{k_2 C_A C_{O2}(a)^2}{(1 + K_A C_A + K_O C_{O2})^2} \quad (2)$$

The formation rates of the unknown by-products P3, P4 and P5 are described with very simple rate equations

$$r_3 = \frac{k_3 C_A C_{O2}(a)^2}{(1 + K_A C_A + K_O C_{O2})^2} \quad (3)$$

$$r_4 = \frac{k_4 C_A C_{O2}(a)^2}{(1 + K_A C_A + K_O C_{O2})^2} \quad (4)$$

$$r_5 = \frac{k_5 C_A C_{O2}(a)^2}{(1 + K_A C_A + K_O C_{O2})^2} \quad (5)$$

In the current work experiments were done under a constant pressure of oxygen, as the focus was on demonstrating feasibility of the reactor concept and comparing different shaped catalysts rather than investigating the influence of oxygen pressure. For the sake of clarity and taking also into account weak adsorption of oxygen on gold the term comprising the adsorption constant of oxygen and its concentration was omitted from the denominator in eq. (1)–(5).

3.4.2. Model for the catalyst layers and the reactor system

The rate equations were implemented in the reaction–diffusion model for the porous catalyst structures. The reaction–diffusion model was used because the experimental results displayed in Fig. 8 indicated strong diffusion limitations inside the extruded catalysts and catalyst foams. The kinetic curve for the powder catalyst is strongly bended, whereas the curves for extrudates and foams are practically straight lines in most cases. This feature is not caused by the lack of dissolved oxygen in the liquid phase, because oxygen was fed into the system in a large excess. The explanation for the form of the kinetic curves for extrudates and foams is thus the internal diffusion limitation. The diffusive flux inside the porous structures is described with the law of Fick,

$$N_i = -D_{ei}\frac{dC_i}{dr} \quad (6)$$

where r is the radial coordinate of the catalyst layer. The mass balance for all organic components and oxygen (i) inside the layer depends on the diffusion flux (N_i) and the reaction rate (r_i) of each component,

$$\varepsilon_P \frac{dC_i}{dt} = -\frac{d(N_i r^s)}{r^s dr} + r_i \rho_P \quad (7)$$

where the general shape factor (s) is a function of the outer surface area and the particle volume,

$$s+1=\left(\frac{A_P}{V_P}\right)R \tag{8}$$

For a cylindrical extrudate with the radius (R) and the length (L) the surface area is $A_P = 2\ \pi R^2 + 2\ \pi RL$ and the volume is $V_P = \pi R^2 L$. The shape factor becomes

$$s=2\left(\frac{R}{L}\right)+1 \tag{9}$$

For the foam, the slab geometry can be assumed and s = 0. Inserting the flux expression (6) in the balance equation (7) gives

$$\varepsilon_P\frac{dC_i}{dt}=\frac{d\left(D_{ei}\frac{dC_i}{dr}r^s\right)}{r^s dr}+r_i\rho_P \tag{10}$$

Assuming that the effective diffusion coefficient (D_{ei}) is constant for each local concentration, the equation, the differentiation of equation (10) gives

$$\varepsilon_P\frac{dC_i}{dt}=D_{ei}\left(\frac{d^2C_i}{dr^2}+\frac{s}{r}\frac{dC_i}{dr}\right)+r_i\rho_P \tag{11}$$

A dimensionless coordinate ($x = r/R$) is introduced,

$$\varepsilon_P\frac{dC_i}{dt}=\frac{D_{ei}}{R^2}\left(\frac{d^2C_i}{dx^2}+\frac{s}{x}\frac{dC_i}{dx}\right)+r_i\rho_P \tag{12}$$

The boundary conditions as well as initial conditions allow the equations to be solved by robust numerical methods, such as the method of lines.

The classical initial and boundary conditions are implemented for the component concentrations inside the particle

$$C_i(t=0)=0, x\in[0,1] \tag{13}$$

$$C_i(t)=C_i'(t), x=1 \tag{14}$$

$$\frac{dC_i}{dx}=0, x=0 \tag{15}$$

Equation (13) tells that the concentrations of the organic components and oxygen are zero in the beginning of the experiment. At the outer surface of the catalyst particle, the concentrations in the pore and in the bulk phase coincide according to equation (14) and in the centre of the layer the concentration gradients vanish according to equation (15). To obtain a very good accuracy for the concentration gradient at the outer surface of the catalyst, numerical integration of the concentration profiles is applied,

$$-\int_0^x d\left(D_{ei}\frac{dC_i}{dr}r^s\right)=\int_0^1 r_i\rho_P(Rx)^s R dx \tag{16}$$

The integration limits for the left-hand side are 0 at x = 0 (as the flux is zero in the particle centre) and $-D_{ei}\ dC_i/dr\ r^s = -D_{ei}\ dC_i/dx\ R^{s-1}$ at x = 1 (i.e. r = R).

Eq. (16) becomes

$$-D_{ei}\frac{dC_i}{dx}R^{s-1}=R^{s+1}\rho_P\int_0^1 r_i x^s dx \tag{17}$$

which is transformed in a straightforward way to

$$-D_{ei}\frac{dC_i}{dx}=R^2\rho_P\int_0^1 r_i x^s dx \tag{18}$$

The flux is at $r = R$

$$N_i=-D_{ei}\frac{dC_i}{dr}=-D_{ei}\frac{dC_i}{Rdx}=R\rho_P\int_0^1 r_i x^s dx \tag{19}$$

The units for the flux Ni and $R\rho_P r_i$ are the same, namely mol/(m^2s).

The liquid circulation rate in the tandem reactor system was high compared to the rates of the chemical reactions, which implies that no concentration gradients appeared inside the reactor. The same approach was considered for temperature gradients, which were neglected because of a negligible difference between the inlet and outlet of the reactor and the latter was supposed to operate in an isothermal mode. Consequently, the reactor system can be described as a single vigorously stirred vessel, which allows a significant simplification of the mathematical treatment. Based on this hypothesis, the mass balance for arabinose, arabinonic acid and the by-products can be written as

$$\frac{dn_i}{dt}=N_i A'_P \tag{20}$$

where A'_P where is the total outer surface of the catalyst particles in the liquid bulk, N_i is the flux at the outer surface of the particles and n_i is the amount of substance (in moles) of each compound. Because the extrudates and solid foams are monodisperse, the total outer surface area can be calculated from the number of catalyst elements and their individual areas

$$A'_P=n_P A_P \tag{21}$$

where the number of catalyst elements are related to the catalyst mass, the density and the element volume,

$$n_P=\frac{m_{cat}}{\rho_P V_P} \tag{22}$$

Consequently, the available surface area becomes

$$A'_P=\frac{m_{cat}(s+1)}{\rho_P R} \tag{23}$$

After inserting the expression (23) in the mass balance (21) the final form is obtained,

$$\frac{dn_i}{dt}=N_i\frac{m_{cat}(s+1)}{\rho_P R} \tag{24}$$

The liquid volume is calculated from the experimental data, taking into account the change of the liquid volume due to the alkali addition and sampling,

$$V(t)=V_0+\int_0^t V'_{added}dt-V_{sampling}(t) \tag{25}$$

The balance equation of gaseous and dissolved oxygen were neglected, because the reactor system was operated under the saturation conditions of oxygen. Thus the concentration of dissolved oxygen is determined by the solubility and the gas–liquid equilibrium constant. Henry's law was applied to describe the gas solubility. The solubility model was adopted from [38].

The model consists of equations (1)–(5), (12)–(15), (17), and (24)–(25). The partial differential equations (12) describing the components inside the catalyst layer were discretized with finite differences. Central differences were used for the first and second derivatives. Thus, a large system of ordinary differential equations (ODEs) was created which was solved with a stiff ODE algorithm, backward difference algorithm implemented in the software Modest [40]. The ODE solver worked under the optimization routine. The model was solved repeatedly and the parameter values were adjusted until the minimum of the objective function (Q)

$$Q=\sum_{i=1}^{n}\sum_{j=1}^{m}\left(C_{expi,j}-C_{esti,j}\right)^2 \tag{26}$$

where n is the number of chemical components and m is the number of time points in the experiment. A combined simplex-Levenberg-Marquardt algorithm was used in the search of the minimum: the parameter estimation was started with the robust simplex algorithm and shifted to the more rapid Levenberg-Marquardt as the optimum was

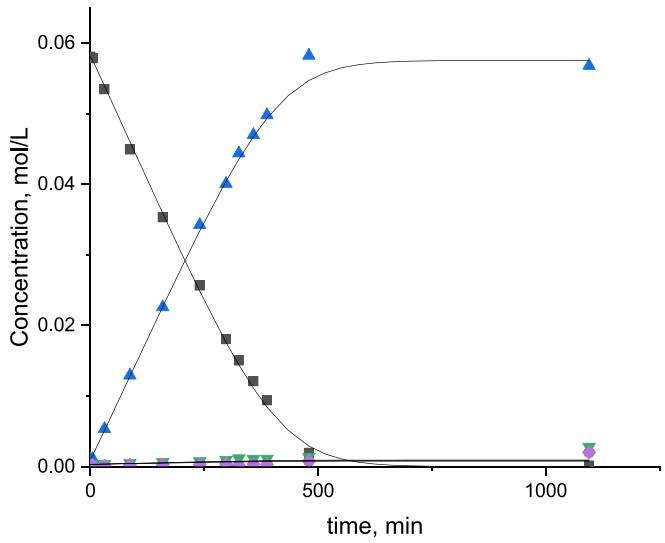

Fig. 10. Kinetic curves (calculated) and experimental data (points) for arabinose oxidation in the tandem reactor system vs time for C6 catalyst. Conditions: 70 °C, pH 8, $pO_2 = 1$ bar. Other details are given in Table 1.

Table 3
The calculated values of reaction parameters for C6 extrudates.

Constant	Unit*	Value	Relative standard error, %
k_1	m^3/min/mol	0.10 10^{-2}	55.5
k_2	m^3/min/mol	0.0455	48.4
k_3	m^3/min/mol	0.33 10^{-3}	98.1
k_4	m^3/min/mol	0.17 10^{-3}	>100
k_5	m^3/min/mol	0.89 10^{-4}	>100
K_A	m^3/mol	0.086	37.3
Catalyst tortuosity	–	4.1	>100

*The units for the rate constants are m^3/min/mol as $\rho_p r_i$ was used in the calculations, implicitly describing dependence on the catalyst amount.

approached.

For illustration purposes the modelling results for the C6 extrudates are given in Fig. 10 with the values of parameters presented in Table 3.

The degree of explanation was 99.78% confirming an excellent correspondence of the model with experiments. The largest standard errors are associated as expected with the rate constants leading to minor components.

4. Conclusions

Oxidation of arabinose over gold on alumina catalyst in the form of extrudates and open cell foams was successfully implemented in a fixed bed reactor under a constant pH of 8, which was ensured by adjusting pH in a CSTR incorporated in the loop. The foam catalysts were prepared by deposition of the catalyst in the powder form containing gold on γ-alumina onto the solid open cell aluminium foams or by deposition precipitation of gold directly on the foam. Alternatively, deposition precipitation was done onto an extruded support. Extrusion of the powder gold/γ-alumina catalyst with γ-alumina and attapulgite or sepiolite as binders was also applied.

Similarly to a batch reactor with Au/Al_2O_3 powder catalyst arabinose was oxidized with a high selectivity into arabinonic acid (90–95%) albeit at a much slower rate, implying mass transfer limitations. Some minor amounts of by-products were also formed under conditions of such limitations. Tested catalysts exhibited very good stability against leaching of gold. For extruded catalysts an effect of the binder type was observed with extrudates with sepiolite displaying higher activity than with attapulgite. Homogeneous deposition–precipitation of gold from its precursor in the presence of urea on shaped catalysts was less efficient in terms of the resulting activity compared to deposition of the catalyst in the form of powder. This could be related to a larger size of gold and less homogeneous distribution of gold particles after the former preparation procedure.

Utilization of a high liquid circulation rate implies a possibility to consider the tandem reactor as a single vigorously stirred vessel simplifying the mathematical treatment. The balance equation of gaseous and dissolved oxygen could be neglected, because the reactor system was operated under the saturation conditions of oxygen. For kinetic modelling the hypothesis of molecularly adsorbed oxygen as the active species in oxidation and the surface reaction between adsorbed oxygen and arabinose as the rate determining step was adopted.

The experimental data for the extruded catalyst obtained in the tandem reactor were successfully modelled giving a high degree of explanation (ca. 99.8%) with the reaction–diffusion model for the porous structures considering the internal mass transfer limitations inside the extruded catalysts and catalyst foams.

Declaration of Competing Interest

The authors declare that they have no known competing financial interests or personal relationships that could have appeared to influence the work reported in this paper.

Data availability

Data will be made available on request.

Acknowledgements

Financial support from Academy of Finland (Academy Professor's grant 319002, T. Salmi, Mobility grant to I. Simakova) is gratefully acknowledged. I. Simakova also acknowledges the financial support of the Ministry of Science and Higher Education of the Russian Federation within the governmental order for Boreskov Institute of Catalysis (project AAAA-A21-121011390055-8).

Appendix A. Supplementary data

Supplementary data to this article can be found online at https://doi.org/10.1016/j.cej.2023.145659.

References

[1] B. Kamm, M. Kamm, P. Gruber, Biorefinery Systems-An Overview, In: *Biorefineries-Industrial Processes and Products. Status Quo and Future Directions*. (Eds: B. Kamm, M. Kamm, P. Gruber), Wiley-VCH, Weinheim 2006, Vol. 1, 3-40.
[2] J.N. Chheda, G.W. Huber, J.A. Dumesic, Angew. Chem. Int. Ed. 46 (2007) 7164–7183.
[3] F. Cherubini, Energ. Conver. Manage. 51 (2010) 1412–1421.
[4] A. Corma, S. Ibora, A. Velty, Chem. Rev. 107 (2007) 2411–2463.
[5] D.Y. Murzin, I.L. Simakova, Catal. Ind. 3 (2011) 218–249.
[6] A.T. Ubando, C.B. Felix, W.-.-H. Chen, Biores Tech. 299 (2020), 122585.
[7] H. Grenman, K. Eränen, J. Krogell, S. Willför, T. Salmi, D.Y. Murzin, Ind. Eng. Chem. Res. 50 (2011) 3818–3828.
[8] J. Rissanen, H. Grenman, C. Xu, S. Willför, D.Y. Murzin, T. Salmi, ChemSusChem 7 (2014) 2947–2953.
[9] R. Rinaldi, F. Schuth, ChemSusChem 2 (2009) 1096–1107.
[10] T. Salmi, D.Y. Murzin, J. Wärnå, P. Mäki-Arvela, B. Kusema, B. Holmbom, S. Willför, AIChE J 60 (2014) 1066–1077.
[11] T. Salmi, D. Murzin, J. Wärnå, P. Mäki-Arvela, B. Kusema, B. Holmbom, S. Willför, Top. Catal. 57 (2014) 1470–1475.
[12] G.C. Bond, C. Louis, D.T. Thompson, Catalysis by Gold, in: G.J. Hutchings (Ed.), Catalysis Science Series, Vol. 6, Imperial College Press, London, 2006.
[13] T. Ishida, N. Kinoshita, H. Okatsu, T. Akita, T. Takei, M. Haruta, Angew. Chem. Int. Ed. 47 (2008) 9265–9268.
[14] A. Mirescu, U. Prüße, Appl. Catal. B: Environ. 70 (2007) 644–652.
[15] B.T. Kusema, B.C. Campo, P. Mäki-Arvela, T. Salmi, D.Y. Murzin, Appl. Catal. A 386 (2010) 101–108.

[16] F. W. Lichtenthaler, The Key Sugars of Biomass: Availability, Present Non-Food Uses and Potential Future Development Lines, in *Biorefineries-Industrial Processes and Products, Status Quo and Future Directions* (Eds: B. Kamm, M. Kamm, P. Gruber), Wiley-VCH, Weinheim, 2006, **2**, 3-59.
[17] B.T. Kusema, B.C. Campo, O.A. Simakova, A.-R. Leino, K. Kordás, P. Mäki-Arvela, T. Salmi, D.Y. Murzin, ChemCatChem 3 (2011) 1789–1798.
[18] L. Correia da Silva, H. Grenman, J. Wärnå, T. Salmi, D.Y. Murzin, Chem. Eng. J. 370 (2019) 952–961.
[19] S. Franz, N.D. Shcherban, I.L. Simakova, M. Peurla, K. Eränen, J. Wärnå, T. Salmi, D.Y. Murzin, React. Kinet. Mech. Catal. 132 (2021) 59–72.
[20] M. Herrero Manzano, K. Eränen, A. Freites Aguilera, J. Wärnå, S. Franz, M. Peurla, J. Garcia Serna, D. Murzin, T. Salmi, Ind. Eng. Chem. Res. 60 (2021) 6483–6500.
[21] O. Simakova, B. Kusema, B. Campo, A.-R. Leino, K. Kordas, V. Pitchon, P. Mäki-Arvela, D.Y. Murzin, J. Phys. Chem. C 115 (2011) 1036–1043.
[22] M. Boronat, A. Corma, Dalton Trans. 39 (2010) 8538–8546.
[23] T.V.W. Janssens, B.S. Clausen, B. Hvolbaek, H. Falsig, C.H. Christensen, T. Bligaard, J.K. Nørskov, Top. Catal. 44 (2007) 15.
[24] M.M. Schubert, S. Hackenbertg, A.C. van Veen, M. Muhler, V. Plzak, J. Behm, J. Catal. 197 (2001) 113.
[25] L.M. Molina, B. Hammer, Appl. Catal. A 291 (2005) 21.
[26] V.A. Sifontes Herrera, O. Oladele, K. Kordas, K. Eränen, J.-P. Mikkola, D.Y. Murzin, T. Salmi, J. Chem. Tech. Biotech 86 (2011) 658–668.
[27] D.Y. Murzin, E.V. Murzina, A. Aho, M. Kazakova, A.G. Selyutin, D. Kubicka, V. L. Kuznetsov, I.L. Simakova, Catal. Sci. Tech. 7 (2017) 5321–5331.
[28] A. Najarnezhadmashhadi, J. Wärnå, K. Eränen, H. Trajano, D. Murzin, T. Salmi, Chem. Eng. Sci. 233 (2021), 116385 (1–10).
[29] G. Araujo Barahona, K. Eränen, D.Y. Murzin, J. Garcia-Serna, T. Salmi, Chem. Eng. Sci. 254 (2022), 117627.
[30] F. van der Klis, L. Gootjes, J. van Haveren, D.S. van Es, J.H. Bitter, React, Chem. Eng. 3 (2018) 540–549.
[31] F. Klis, L. Gootjes, N.H. Verstijnen, D.S. van Es, J.H. Bitter, RSC Adv. 12 (2022) 8918–8923.
[32] A. Padovani, Glucose oxidation into gluconic acid: from batch to trickle bed reactor, Ruhr-Universität Bochum, Bochum, 2016. PhD thesis.
[33] I. Simakova, Z. Vajglová, P. Mäki-Arvela, K. Eränen, L. Hupa, M. Peurla, E. Mäkilä, J. Wärnå, D.Y. Murzin, Org. Proc. Res. Devel. 26 (2022) 387–403.
[34] I. Simakova, P. Mäki-Arvela, M. Martinez-Klimov, J. Muller, Z. Vajglová, M. Peurla, K. Eränen, D.Y. Murzin, One-pot synthesis of menthol starting from citral over Ni supported on attapulgite-H-beta-38 extrudates in a continuous flow: effect of metal location, Ind. Eng. Chem. Res. 61 (2022) 12998–13010.
[35] T. Haakana, E. Kolehmainen, I. Turunen, J.-P. Mikkola, T. Salmi, Chem. Eng. Sci. 59 (2004) 5629–5635.
[36] Y.S. Demidova, I.L. Simakova, M. Estrada, S. Beloshapkin, E.V. Suslov, D. V. Korchagina, K.P. Volcho, N.F. Salahutdinov, A.V. Simakov, D.Y. Murzin, Appl. Catal. A 464–465 (2013) 348–356.
[37] G. Araujo Barahona, K. Eränen, J.P. Oña, D.Yu. Murzin, J. Garcia-Serna, T. Salmi, *Ind. Eng. Chem. Res.*, **2022**, *61*, 2734-2747.
[38] B. Worgul, A. Freites Aguilera, C. Vergat-Lemercier, K. Eränen, O. Simakova, H. Held, H. Freund, D.Y. Murzin, T. Salmi, Chem. Eng. Sci. 260 (2022), 117948.
[39] A. Aho, S. Engblom, K. Eränen, V. Russo, P. Mäki-Arvela, N. Kumar, J. Wärnå, T. Salmi, D.Y. Murzin, Chem. Eng. J. 405 (2021), 126945 (1–14).
[40] H. Haario, ModEst, Modelling and Estimation Software, Profmath, Helsinki, 2022.